

Specification, implementation, and hardware-in-the-loop real-time simulation of an active distribution grid[☆]



H. Hooshyar^{a,*}, F. Mahmood^a, L. Vanfretti^{a,b}, M. Baudette^a

^a KTH Royal Institute of Technology, Stockholm, Sweden

^b Statnett SF, Oslo, Norway

ARTICLE INFO

Article history:

Received 4 August 2014

Received in revised form

26 May 2015

Accepted 28 June 2015

Available online 21 July 2015

Keywords:

Active distribution network

Dynamic performance

Real-time

Hardware-in-the-loop

PMU

OPAL-RT

ABSTRACT

This paper presents the IDE4L project reference grid model developed to serve as a benchmark for studies on distribution grid dynamics within the project. The paper demonstrates a MATLAB/Simulink implementation of the reference grid to be used in real-time hardware-in-the-loop simulations. The simulations will be carried out to study distribution grid dynamics and to evaluate the techniques developed in IDE4L project for TSO/DSO interactions. Performance of the grid model is shown through sample real-time simulation results and a hardware-in-the-loop setup for PMU-based grid monitoring applications.

© 2015 The Authors. Published by Elsevier Ltd.

This is an open access article under the CC BY-NC-ND license (<http://creativecommons.org/licenses/by-nc-nd/4.0/>).

1. Introduction

FUNDED by the European Commission's FP7 program (7th FRAMEWORK Program for Research and Technological Development), the IDE4L (Ideal Grid for All) project has recently started to define, develop and demonstrate distribution grid automation system, IT platform and applications for active distribution grid management [1]. The project is composed of several work packages to cover different aspects of active grid management. As part of work package 6 of the project, tighter integration of the operation of transmission grids (HV) with distribution grids (MV and LV) through exchange of key dynamic information between TSOs and DSOs will be investigated. The key information exchange will be performed by coupling the use of PMU data from HV, MV, and LV grids, coherently. To demonstrate such tight interaction and also to evaluate the quality and relative merits of the developed techniques, there is a need to develop a reference distribution grid

model that includes a distribution grid (MV and LV) and also parts of the transmission grid (HV). The model will be then coupled together with PMUs, external controllers, and a co-simulation of communication networks to carry out real-time hardware-in-the-loop simulation studies.

The proposed test grids in the literature often operate at single voltage levels and also lack components such as distributed generators and protection systems, so they cannot fulfill the requirements for studies in the IDE4L project [2–4].

This paper develops specifications for an active distribution grid model to be used for this purpose. The model is implemented in MATLAB/Simulink and modified for its use with the OPAL-RT real-time simulator. The grid topology is based on Roy Billinton Transmission Test System and IEEE standard test feeders, including HV, MV and LV voltage levels.

In the next section, the paper introduces the developed components that are incorporated in the grid model in Section 3 where the grid specifications are explained. Section 4 elaborates on real-time simulation of the grid model and illustrates a hardware-in-the-loop setup prepared for grid monitoring applications via PMU measurements. Conclusions and future work are listed in Section 5.

2. Models of components

This section illustrates the developed components for the reference grid model. The components will be used in the next section to be incorporated in the overall grid model.

[☆] This work was supported in part by the FP7 IDE4L project funded by the European Commission, the STandUp for Energy Collaboration Initiative and by Statnett SF, the Norwegian TSO.

* Corresponding author.

E-mail addresses: hossein.hooshyar@ee.kth.se (H. Hooshyar), farhan.mahmood@ee.kth.se (F. Mahmood), luigi.vanfretti@ee.kth.se, luigi.vanfretti@statnett.no (L. Vanfretti), maxime.baudette@ee.kth.se (M. Baudette).

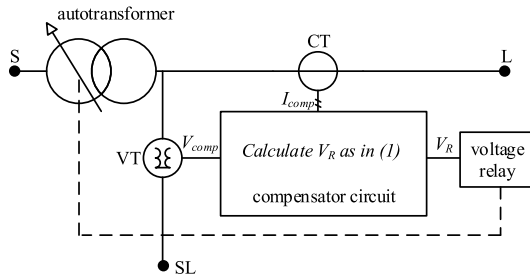


Fig. 1. Conceptual diagram of the developed VR component.

2.1. Single-phase step voltage regulator (VR)

The single-phase VR is implemented based on the model reported in [5]. The model consists of an autotransformer and a step voltage regulating relay that governs a load tap-changing mechanism, as illustrated in Fig. 1. Table 1 lists input parameters of the developed component.

The position of the tap is controlled by the compensator circuit through manipulating the input of the regulating relay as shown in (1):

$$V_R = V_{comp} - (R_c + jX_c)I_{comp} = V_{comp} - (R_{comp} + jX_{comp}) \quad (1)$$

where V_R is the input to the regulating relay, and V_{comp} and I_{comp} are the VT secondary voltage and the CT secondary current, respectively. R_c and X_c represent the per-unit equivalent line impedance from the regulator output to the regulation point. Note that in practice, the compensator settings, R_{comp} and X_{comp} , are expressed in units of volts as R_{comp} and X_{comp} are defined as $R_c I_{comp}$ and $X_c I_{comp}$, respectively.

The component contains a reversing switch enabling a $\pm 10\%$ regulating range, in 16 steps up and 16 steps down. The regulating relay performs a tap change if:

$$V_R - V_{ref} > BW/2 \text{ during a time } t > T_d. \quad (2)$$

Note that the logic delay can vary from 1 s to hundreds of seconds and is determined by the system operator based on the feeder operating conditions. Having different logic delays results in different system dynamics.

2.2. Static load

In this study, “static loads” are referred to loads that do not contain any motor. Table 2 lists the input parameters of the developed component. The component has been developed in two versions of single-phase and three-phase. It can be chosen to be either constant current, constant impedance or constant power load; however, if the load terminal voltage drops to less than the “Operational minimum voltage”, the model changes to a constant impedance load.

Fig. 2 illustrates the conceptual diagram of the developed component. As shown, the load is modeled as a controlled current source whose current is calculated based on V , which is the terminal line-to-ground voltage for single-phase loads or the terminal line-to-ground positive sequence voltage for three-phase loads, and P and Q , which are active and reactive power of the load. P and Q are calculated as:

$$P = P_n \left(\frac{V}{V_n} \right)^{NP} + \underbrace{P_n P_{sin} \sin(2\pi f_P t)}_* + \underbrace{P_n S_{rand} Rand}_{**} \quad (3)$$

$$Q = Q_n \left(\frac{V}{V_n} \right)^{NQ} + \underbrace{Q_n Q_{sin} \sin(2\pi f_Q t)}_* + \underbrace{Q_n S_{rand} Rand}_{**} \quad (4)$$

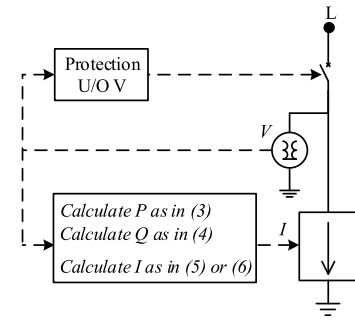


Fig. 2. Conceptual diagram of the developed static load component.

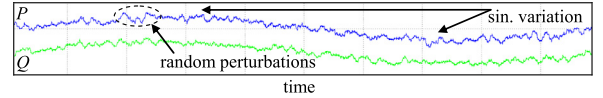


Fig. 3. Static load random perturbations and sinusoidal variation.

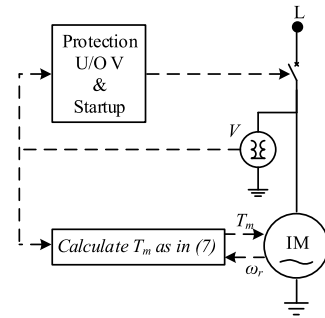


Fig. 4. Conceptual diagram of the developed dynamic load component.

where t is the simulation time. * and ** are two additional terms, added to the base power, representing load slow variations and random switchings occurring inside the model (as the model may be an aggregation of small loads), respectively. The impact of these additional terms is depicted in Fig. 3. $Rand$ is a function that generates uniformly distributed pseudorandom numbers between 0 and 1. Note that NP and NQ are both 0 for constant power, 1 for constant current, and 2 for constant impedance loads [6].

The load current, I , is obtained from (5) for single-phase loads and from (6) for three-phase loads.

$$I = (P + jQ) / V^* \quad (5)$$

$$\begin{cases} I_a = (P + jQ) / 3 / V^* \\ I_b = I_a e^{-j2\pi/3} \\ I_c = I_a e^{j2\pi/3} \end{cases} \quad (6)$$

Also, as shown in Fig. 2, an over/under voltage protection scheme is employed for the model which can be adjusted through protection settings. If the load is tripped, it reconnects to the grid provided that the grid voltage remains in the permissible range for at least the “Reconnection time”.

2.3. Dynamic load

We refer to “dynamic loads” as loads that have an induction motor. Table 3 lists the input parameters of the developed component. The component has been developed in two versions of single-phase and three-phase. As shown in Fig. 4, the heart of the model is an induction motor whose mechanical load torque is modeled as [7]:

$$T_m = \begin{cases} 0.85 + 0.15\omega_r^4 \text{ p.u., non-stall condition} \\ 20 \text{ p.u., stall condition.} \end{cases} \quad (7)$$

Table 1
Input parameters of VR component.

	Parameter	Description	Value (as an example)
Basics	S_n	Nominal power	5 MVA
	f_n	Nominal frequency	50 Hz
	V_n	Nominal voltage	20 kV-RMS
	I_n	Rated feeder current	200 A
Regulation	V_{ref}	Reference voltage	1.016 p.u.
	BW	Bandwidth	0.016 p.u.
	T_d	Time delay (logic delay + mechanical delay)	4 s (1 s + 3 s)
Compensator	R_{comp}	Compensator setting	2.7 V
	X_{comp}	Compensator setting	1.6 V

Table 2
Input parameters of static load component.

	Parameter	Description	Value (as an example)
Basics	$Type$	Load type	Constant power, constant current, constant impedance
	P_n	Nominal active power	16 kW
	Q_n	Nominal reactive power	8 kVAr
	f_n	Nominal frequency	50 Hz
	V_n	Nominal voltage	20 kV-RMS
	V_{omv}	Operational minimum voltage	0.7 p.u.
Load change	S_{rand}	Gain of random power perturbations	0.05 p.u.
	P_{sin}	Gain of sinusoidal active power variation	0.01 p.u.
	Q_{sin}	Gain of sinusoidal reactive power variation	0.01 p.u.
	f_p	Frequency of sinusoidal active power variation	0.03 Hz
	f_Q	Frequency of sinusoidal reactive power variation	0.03 Hz
Protection	V_{min}	Minimum voltage	0.8 p.u.
	V_{max}	Maximum voltage	1.2 p.u.
	t_{trip}	Trip time	1 s
	t_{rec}	Reconnection time	10 s

Table 3
Input parameters of dynamic load component.

	Parameter	Description	Value (as an example)
Basics	S_n	Nominal power	7.5 kVA
	f_n	Nominal frequency	50 Hz
	V_n	Nominal voltage	3.8 kV-RMS
	t_{start}	Start time	30 s
	V_{omv}	Operational minimum voltage	0.65 p.u.
	t_{stall}	Stalling period	20 s
Induction motor	$[R_s, L_s]$	Stator resistance and inductance	[0.01965, 0.0397] p.u.
	$[R_r', L_r']$	Rotor resistance and inductance	[0.01909, 0.0397] p.u.
	L_m	Mutual inductance	1.354 p.u.
	H	Inertia constant	0.09526 s
	F	Friction factor	0.05479 p.u.
	p	Pole pairs	2
Protection	V_{min}	Minimum voltage	0.8 p.u.
	V_{max}	Maximum voltage	1.2 p.u.
	t_{trip}	Trip time	1 s
	t_{rec}	Reconnection time	10 s

Standard Simulink asynchronous machine blockset, modeled based on [8] representing the electrical part of the machine by a fourth-order state-space model and the mechanical part by a second-order system, has been used to represent the induction motor. Extra logic has been added to make the motor stall for the “Stalling period” if the load terminal voltage drops to less than the “Operational minimum voltage”. It is also possible to set a start time at which the load will be switched on. Note that an over/under voltage protection scheme is employed for the model which can be adjusted through protection settings. Similar to the static load components, the dynamic load reconnects to the grid after being tripped, provided that the grid voltage remains in the permissible range for at least the “Reconnection time”.

2.4. Wind farm

The wind farm component was built starting from the doubly-fed induction generator (DFIG) based wind turbine model developed by OPAL-RT that uses average models for the converters [9].

Fig. 5 illustrates the conceptual diagram of the wind farm component. The DFIG is modeled using the Simulink asynchronous machine blockset, as used in dynamic load component. The wind turbine model, obtained based on the steady-state power characteristics of the turbine [10], is adopted from the standard Simulink variable pitch wind turbine model. The control system generates the pitch angle command and the voltage command signals, V_r and V_{inv} , in order to control the power of the wind

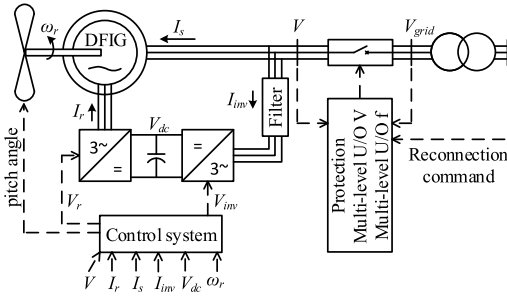


Fig. 5. Conceptual diagram of the developed wind farm component.

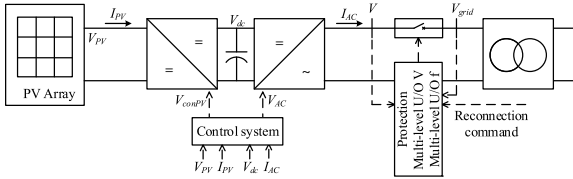


Fig. 6. Conceptual diagram of the developed PV farm component.

turbine, the DC bus voltage and the reactive power or the voltage at the grid terminals. The DC-link voltage controller is a vector controller that permits keeping constant the DC-link voltage level. The rotor-side controller is a stator flux based vector controller that enables independent control of the induction machine active and reactive powers [11].

As shown in Fig. 5, a multilevel U/O voltage/frequency protection scheme with ride-through capability for temporary faults is added to the model against faults occurring on the grid. Note that, in contrast to the load models that can independently reconnect to the grid, reconnection of such plants is coordinated by the distribution grid control center through the “Reconnection command” signal.

The whole model has been masked to form a component in Simulink. Table 4 lists the input parameters of the developed component. The nominal output of the component for average wind speed of 15 m/s is 1.5 MW which is scalable by the “Number of wind turbines”.

Note that the wind speed pattern can be adjusted in two types of constant or repeating sequence of time-value pairs.

2.5. PV farm and residential PV system

The PV component is a grid connected PV system that is simulated by adopting a model which represents the converters with average value models and includes maximum power point tracker (MPPT) [12].

The component has been developed in two versions of single-phase, representing residential PV systems, and three-phase, representing PV farms. Fig. 6 illustrates the conceptual diagram of the developed model. The control system consists of an inverter controller which regulates V_{dc} at its reference value, and a Perturb & Observe MPPT which generates converter voltage command signal to vary the operating point of PV modules so that the modules are able to deliver maximum available power.

As shown in Fig. 6, a multilevel U/O voltage/frequency protection scheme with ride-through capability for temporary faults is added to the model against faults occurring on the grid. For PV farm model, the reconnection of the model is coordinated by the distribution grid control center through the “Reconnection command” signal; however, for residential PV system model, reconnection is performed independently by the model provided that the grid voltage and frequency remains in the permissible range for

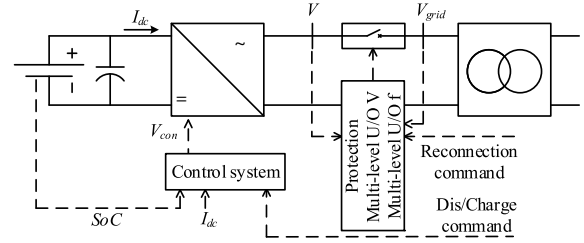


Fig. 7. Conceptual diagram of the developed CES component.

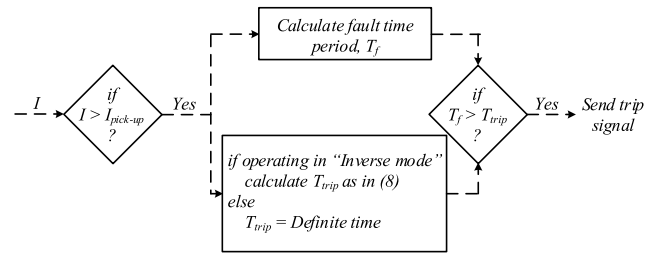


Fig. 8. Conceptual diagram of the developed overcurrent relay model.

at least the “Reconnection time”. Also, protection settings for residential PV system model are pre-adjusted according to IEEE 929 Standard [13].

The whole model has been masked to form a component in Simulink. Table 5 lists the input parameters of the developed component. The nominal outputs of the PV farm and residential PV system components for constant solar irradiation of 1000 W/m² are 100 kW and 10 kW, respectively. The outputs are scalable by the “Number of PV systems”.

Note that the solar irradiation pattern can be adjusted in two types of constant or repeating sequence of time-value pairs.

2.6. Community energy storage (CES)

The CES component is a grid connected inverter-interfaced battery storage model. The converters are represented with average value models.

Fig. 7 illustrates the conceptual diagram of the developed component. The battery model, obtained based on characteristics of Nickel-Metal-Hydrate batteries [14], is adopted from the standard Simulink battery blockset. As shown in the figure, charging/discharging rate of the model is controlled by “Dis/Charge command” coming from the distribution grid control center. The control system consists of a lower level control which regulates the power being charged or discharged, and an upper level control which monitors the SoC (State of Charge) of the battery and stops the charging/discharging process if the SoC goes beyond the permissible range that is specified in Table 6 [15].

The same multilevel U/O voltage/frequency protection scheme with ride-through capability, employed for PV farm and wind farm components, is employed for this model. Similarly, the reconnection command comes from the distribution grid control center.

2.7. Feeder overcurrent protection (FOP)

The FOP component consists of a phase overcurrent relay monitoring feeder phase currents and a ground overcurrent relay monitoring feeder current zero-sequence component.

Fig. 8 illustrates the conceptual diagram of the developed overcurrent relay model. The overcurrent relay model can operate under two modes of operation, “Inverse” or “Definite”. In case of

Table 4
Input parameters of wind farm component.

	Parameter	Description	Value (as an example)
Wind farm	N_{WT}	Number of wind turbines	33
	f_n	Nominal frequency	50 Hz
	V_n	Nominal L–L voltage	36 kV-RMS
Induction generator	$[R_s, L_s]$	Stator resistance and inductance	[0.00706, 0.171] p.u.
	$[R_r', L_r']$	Rotor resistance and inductance	[0.005, 0.156] p.u.
	L_m	Mutual inductance	2.9 p.u.
	H	Inertia constant	5.04 s
	F	Friction factor	0.01 p.u.
DC link	p	Pole pairs	3
	V_{dc}	Nominal voltage of DC link	1440 V
Control system	C_{dc}	DC link capacitor	10 mF
	Kp_{pa}	Pitch angle controller gain	500
	PA_{max}	Maximum pitch angle	45°
	$[Kp_{VAr}, Ki_{VAr}]$	Reactive power regulator gains	[0.05, 5]
	$[Kp_{dc}, Ki_{dc}]$	DC bus voltage regulator gains	[0.002, 0.05]
	$[Kp_{gr}, Ki_{gr}]$	Grid-side converter current regulator gains	[2.5, 500]
	$[Kp_{rt}, Ki_{rt}]$	Rotor-side converter current regulator gains	[0.3, 8]
Wind	$Type$	Type of wind speed	Constant, time series
	W_c	Constant speed average	15 m/s
	W_{ts}	Wind speed series	[4 8 11 15] m/s
	T_{ts}	Wind time series	[0 75 90 175] s
Protection	$[V_{min2}, V_{min1}, V_{max1}, V_{max2}]$	Voltage levels	[0.5, 0.88, 1.1, 1.3] p.u.
	$[V < V_{min2}, V_{min2} < V < V_{min1}, V_{max1} < V < V_{max2}, V_{max2} < V]$	Trip times for voltage protection	[0.24, 4.8, 4.8, 0.24] s
	$[f_{min}, f_{max}]$	Frequency levels	[49.3, 50.5] Hz
	$[f < f_{min}, f_{max} < f]$	Trip times for freq. protection	[0.24, 0.24] s

Table 5
Input parameters of PV farm/residential PV components.

	Parameter	Description	Value (as an example)
PV system	N_{PV}	Number of PV systems	6
	f_n	Nominal frequency	50 Hz
	V_n	Nominal voltage	3.8 kV-RMS
PV module	I_{sc}	Short-circuit current	3.83 A
	V_{oc}	Open-circuit voltage	68.7 V
	I_r	Current at P_{max}	3.59 A
	V_r	Voltage at P_{max}	55.8 V
	N_{series}	Number of modules in series	4
	N_{shunt}	Number of modules in parallel	1
DC link	V_{dc}	Nominal voltage of DC link	500 V
	C_{dc}	DC link capacitor	200 μ F
Control system	$[Kp_{VAr}, Ki_{VAr}]$	V_{dc} regulator gains	[0.01, 0.01]
	T_{sample}	MPPT sample interval	0.01 s
	$deltal$	MPPT current increment	0.01 A
Solar irradiation	$Type$	Type of solar irradiation	Constant, time series
	SI_c	Constant solar irradiation	1000 W/m ²
	SI_{ts}	Solar irradiation series	[0 800 1000 800 0] W/m ²
Protection	T_{ts}	Wind time series	[0 100 200 300 400] s
	$[V_{min2}, V_{min1}, V_{max1}, V_{max2}]$	Voltage levels (only for PV farm model)	[0.5, 0.88, 1.1, 1.3] p.u.
	$[V < V_{min2}, V_{min2} < V < V_{min1}, V_{max1} < V < V_{max2}, V_{max2} < V]$	Trip times for voltage protection (only for PV farm model)	[0.24, 4.8, 4.8, 0.24] s
	$[f_{min}, f_{max}]$	Frequency levels (only for PV farm model)	[49.3, 50.5] Hz
	$[f < f_{min}, f_{max} < f]$	Trip times for frequency protection (only for PV farm model)	[0.24, 0.24] s
	t_{rec}	Reconnection time (only for residential PV system model)	10 s

“Inverse”, trip time is obtained from:

$$T_{trip} = TD \left(a + \frac{b}{(I/I_{pick-up})^c - 1} \right) \quad (8)$$

where TD is the time dial and $I_{pick-up}$ is the pick-up current. a , b , and c are constants forming the relay operative curve.

The relay performs three reclosing attempts before it locks out. Time intervals between reclosing attempts can be adjusted through input parameters as listed in Table 7. Two operative curves can be embedded in the model; one for the first operation, often

set to be faster for the purpose of fuse-saving, and one for the next three operations, often set to be slower [16].

2.8. Three-phase and single-phase recloser

The developed three-phase recloser component is composed of a phase and a ground overcurrent relay, introduced in the previous section, and a three-phase breaker; hence, it has three-phase operation. The single-phase recloser component consists of a phase overcurrent relay monitoring one phase current and a single-phase

Table 6
Input parameters of CES component.

	Parameter	Description	Value (as an example)
CES system	S_{inv}	Nominal inverter rating	150 kVA
	f_n	Nominal frequency	50 Hz
	V_n	Nominal L-L voltage	6.6 kV-RMS
Battery	Ah	Total battery storage capacity	200 Ah
	SoC_{min}	Minimum SoC	20%
	SoC_{max}	Maximum SoC	90%
Control system	$[Kp, Ki]$	Power regulator gains	[0.5, 50]
Protection	$[V_{min2}, V_{min1}, V_{max1}, V_{max2}]$	Voltage levels	[0.5, 0.88, 1.1, 1.3] p.u.
	$[V < V_{min2}, V_{min2} < V < V_{min1}, V_{max1} < V < V_{max2}, V_{max2} < V]$	Trip times for voltage protection	[0.24, 4.8, 4.8, 0.24] s
	$[f_{min}, f_{max}]$	Frequency levels	[49.3, 50.5] Hz
	$[f < f_{min}, f_{max} < f]$	Trip times for frequency protection	[0.24, 0.24] s

Table 7
Input parameters of feeder overcurrent protection component.

	Parameter	Description	Value (as an example)
Basics	f_n	Nominal frequency	50 Hz
	Mode	Mode of operation	Definite, Inverse
	$T_{interval}$	Open intervals between reclosing attempts	[0.25 15 35]
First operation	$[a, b, c]$	Operative curve constants	[0.0 0.14 0.02]
	$I_{pick-up}$	Pick-up current	140
	TD	Time dial	0.01
	$T_{definite}$	Definite time (will be used only if operating mode is selected as “Definite”)	0.2
Next operations	$[a, b, c]$	Operative curve constants	[0.0 0.14 0.02]
	$I_{pick-up}$	Pick-up current	140
	TD	Time dial	0.05
	$T_{definite}$	Definite time (will be used only if operating mode is selected as “Definite”)	0.4

breaker; hence, it has single-phase operation. Input parameters of the components are the same as those of the overcurrent relay model.

2.9. Electric power system (EPS)

The EPS component is developed to incorporate the dynamics of the HV grid. The heart of the component is a synchronous generator together with steam turbine and governor, excitation system, and PSS models, as illustrated in Fig. 9. Standard Simulink synchronous machine blockset, modeled based on [8] representing the electrical part of the machine by a sixth-order state-space model, has been used to represent the synchronous generator. The steam turbine and governor model is implemented base on [17] and contains a single-mass tandem-compound steam prime mover system including speed regulator, steam turbine and a shaft. The excitation system model implements an IEEE Type 1 synchronous machine voltage regulator combined to an exciter [18]. The Power System Stabilizer (PSS) model is added to damp the rotor oscillations of the synchronous machine by controlling its excitation. The input of the PSS model is synchronous machine speed deviation with respect to its nominal value ($d\omega$). It consists of a low-pass filter, a general gain, a washout high-pass filter, a phase-compensation system, and an output limiter [19].

Table 8 lists the input parameters of the developed component. Values for input parameters of synchronous generator, steam turbine and governor, excitation system, and PSS models have been adopted from Example 12.6, pp. 813 of [19].

Note that since the system total generation can be different from the power demanded by the grid connected to the EPS component ports, a constant power load, specified as “System load” in Fig. 9, is included in the EPS model to represent the rest of the power system loads and to absorb the power difference between the total nominal generation and the “initial consumption” of the connected grid. The “System load” power remains constant during

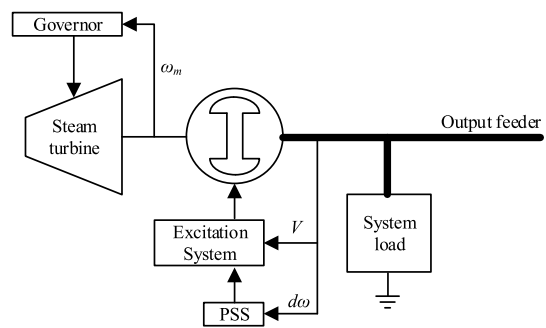


Fig. 9. Conceptual diagram of the developed EPS component.

the simulation and any change in the connected grid consumption triggers the governor model to regulate the power generated by the synchronous generator model.

3. The reference distribution grid model

This section introduces the reference distribution grid topology and describes how the component models, developed in Section 2, are incorporated in the grid model.

3.1. Specifications of the model

Fig. 10 depicts the single-line diagram of the reference distribution grid model. As the figure shows, the grid model includes four different sections: HV (220 kV), MV (36 kV), LV (6.6 kV), and residential LV (0.4 kV). Although the HV section is not considered to be part of the modeled distribution grid, it is included in the model to incorporate the dynamics of the HV grid. The whole model is implemented in MATLAB Simulink.

The HV section consists of an EPS model and a 6-bus network adopted from the Roy Billinton Transmission Test System

Table 8
Input parameters of EPS component.

	Parameter	Description	Value (as an example)	
Synchronous generator	V_n	Nominal L–L voltage	230 kV-RMS	
	f_n	Nominal frequency	50 Hz	
	S_{gen}	Total generation	1000 MVA	
	H	Inertia coefficient	6.5 s	
	$[X_d, X_d', X_d'', X_q, X_q', X_q'', X_l]$	Reactances	[1.8, 0.3, 0.25, 1.7, 0.55, 0.25, 0.2] p.u.	
	$[T_{do}, T_{do}', T_{qo}, T_{qo}']$	Time constants	[8, 0.03, 0.4, 0.05] s	
	R_s	Stator resistance	0.0025 p.u.	
	p	Pole pairs	4	
	Steam turbine and governor	Kp	Regulator gain	1
		$[R_p, D_z]$	[permanent droop, dead zone]	[0.05, 0] p.u.
$[T_{sr}, T_{sm}]$		[speed relay, servo-motor] time constant	[0.001, 0.15] s	
$[v_{g_{min}}, v_{g_{max}}, g_{min}, g_{max}]$		Gate opening limits	[-0.1 (p.u./s), 0.1 (p.u./s), 0 (p.u.), 4.496 (p.u.)]	
ω_m		Nominal speed of synchronous machine	3600 rpm	
$[T_2, T_3, T_4, T_5]$		Steam turbine time constants	[0, 10, 3.3, 0.5] s	
$[F_2, F_3, F_4, F_5]$		Turbine torque fractions	[0, 0.36, 0.36, 0.28]	
P_{m0}		Initial power	0.141 p.u.	
Excitation system		T_r	Low-pass filter time constant	0.02 s
		$[K_a, T_a]$	Regulator gain and time constant	[200, 0.001 s]
	$[K_e, T_e]$	Exciter gain and time constant	[1, 0 s]	
PSS	T_{sensor}	Sensor time constant	0.015 s	
	K_{PSS}	Gain	30	
	T_{wash}	Wash-out time constant	10 s	
	$[T_{num1}, T_{den1}]$	Lead–lag #1 time constants	[0.05, 0.02] s	
	$[T_{num2}, T_{den2}]$	Lead–lag #2 time constants	[3, 5.4] s	
	$[V_{S_{min}}, V_{S_{max}}]$	Output limits	[-0.15, 0.15] p.u.	

(RBTS) [20]. Since the model will be used in a European project, the system voltage is reduced from the original 230 to 220 kV to comply with the European voltage levels [21]. The transmission line sections are modeled with PI sections using sequence impedances except line section 100–101 which is modeled by ARTEMiS distributed parameters line block. They will be better explained in Section 4.1. As shown in Fig. 10, a 50 MW wind farm generation is added to the HV section. Values of input parameters for all lines and components are listed in the Appendix A.

The MV section topology is based on the IEEE 34 bus test feeder. Values of parameters for all feeder sections precisely follow the test feeder data in [2]; therefore they are not repeated in this paper. As the distribution feeder sections are unbalanced, meaning that self-impedances and self-susceptances of different phases and also mutual impedances and susceptances between different pairs of phases are not the same, it is not possible to model them with PI sections. Instead, as illustrated in Fig. 11, a MATLAB Simulink mutual inductance component, implementing a full 3×3 impedance matrix, together with 12 capacitors, implementing a full 3×3 susceptance matrix, is used to model each feeder section. The system voltage is increased from the original 24.9 to 36 kV, a European voltage level. As shown in Fig. 10, three constant power loads (total of 110 kVA) are replaced by dynamic load models to incorporate motor loads dynamics. Also, two 1.5 MW wind farm model is added to the middle and to the end of the feeder. Since the original test feeder lacks any protection system, a circuit breaker supervised by an overcurrent protection block and a three-phase recloser are added to the beginning and to the middle of the MV feeder, respectively. Values of input parameters for all components are listed in the Appendix A.

The LV and residential LV sections are built based upon the IEEE 37 bus test feeder. Similar to the MV section, values of parameters for all feeder sections are set precisely according to the test feeder data in [2]; therefore they are not repeated in this paper. The same approach used to model MV feeder sections is used for modeling the LV feeder sections. The system voltage levels have been changed to comply with European voltage levels: for LV, from 4.8 to 6.6 kV, and for residential LV, from 0.48 to 0.4 kV. As shown in Fig. 10, two constant power loads (total of 150 kVA)

are replaced by dynamic load models. Also, two PV farm models (total of 1.05 MW), three residential PV system models (total of 0.77 MW), two CES models (total of 325 Ah), and two sets of single-phase recloser are added to this section. Note that the relatively high generation of residential PV models is because these models represent aggregation of residential PV systems. Values of input parameters for all components are listed in the Appendix A.

Finally, note that, as a result of having several components connected to the grid model, it is quite difficult to initialize the grid model in an equilibrium operating point. Observe that real-time software applications such as MATLAB/Simulink for Opal-RT do not contain three-phase unbalanced power flow. As our model represents a distribution grid, it is highly unbalanced. Therefore it was not possible to use Simulink embedded power flow for our grid model. So, two auxiliary ideal voltage sources, connected at nodes 104 and 890/799, are used at the simulation startup to help the grid model to reach to a stable operating point. The ideal voltage sources are then disconnected after the first 10 s of simulation.

3.2. Settings and coordination of protective devices

In order to adjust settings and to coordinate the added feeder protective relays and reclosers, required fault analysis study, following the methodology reported in [22], was conducted. It is worth noting that the study is performed assuming there is no distributed generation connected to the grid. This is to observe the impact of the added distributed generation on the performance of the protection system.

Figs. 12 and 13 show the curves selected for phase relays. Selected curves for ground relays are not shown here. As the figures show, the MV feeder protective relay is coordinated with downstream MV and LV reclosers. Also, the LV reclosers are coordinated with each other. Values of input parameters of all phase and ground relays are listed in the Appendix A.

Note that as fault current levels are different in MV and LV sections, per unit values of fault currents were used in the time–current curves for relay coordination studies. The minimum safety factor, considered between trip times of two consecutive relays against the maximum fault current flowing through both of them, is 0.1 s.

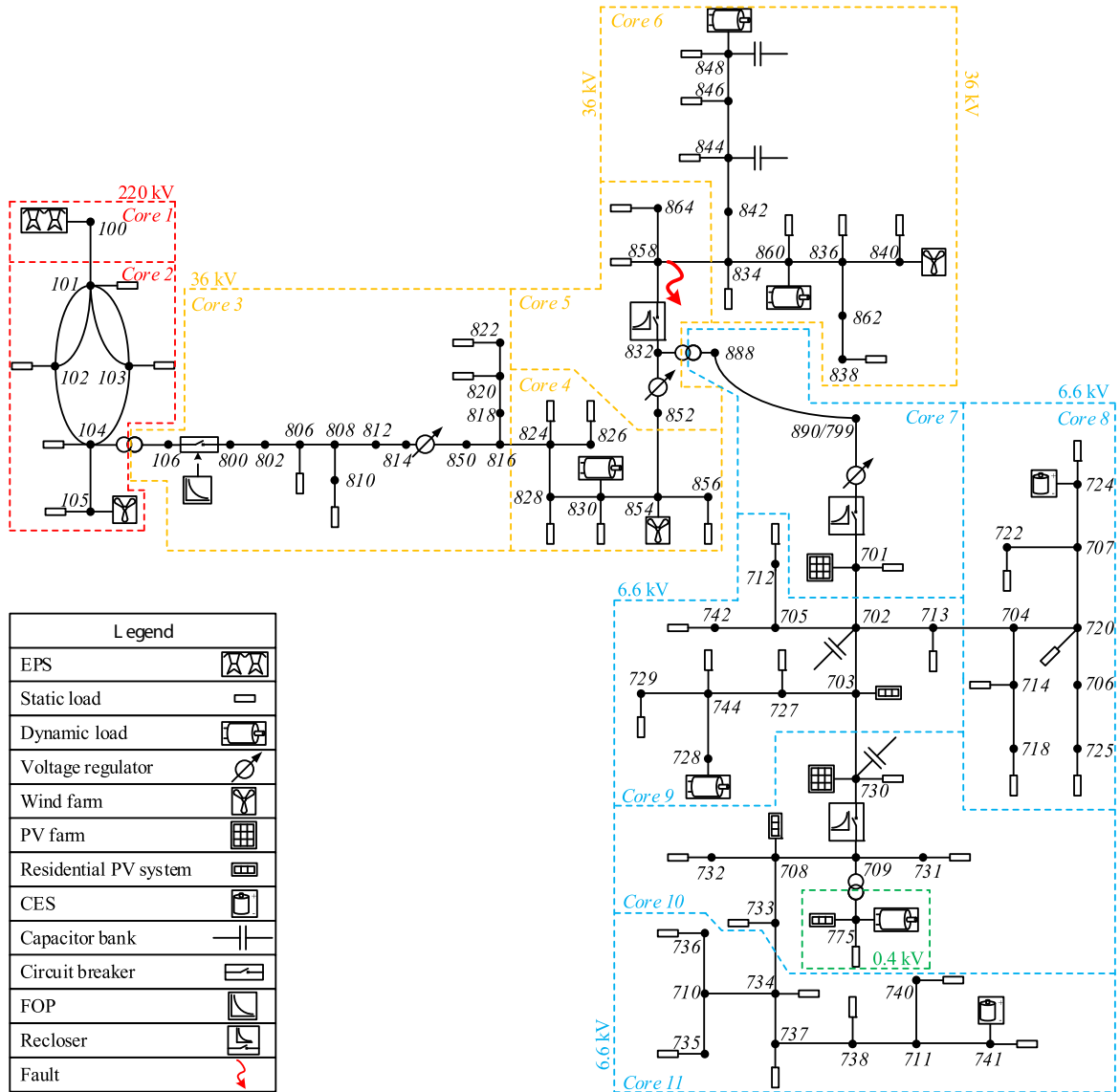


Fig. 10. Single-line diagram of the reference distribution grid model.

4. Hardware-in-the-loop real-time simulation

This section elaborates on real-time simulation of the grid model, developed in the previous section, and illustrates a hardware-in-the-loop setup prepared for grid monitoring applications via PMU measurements. Note that algorithms, to be developed during the IDE4L project, for exchange of key dynamic information between TSOs and DSOs will be added to this setup for evaluation and demonstration purposes.

4.1. Model setup for real-time simulation

Due to high computational burden of the grid model, parallel distributed computing capability embedded in OPAL-RT's simulator has been utilized to comply with real-time simulation constraints. Hence, as shown in Fig. 10, the grid model is distributed into total of 11 cores of the OPAL-RT simulator (HV section into 2 cores, MV section into 4 cores, and LV and residential LV sections into 5 cores).

Splitting the grid model into 11 sub-models has been done by utilizing ARTEMiS distributed parameters line block, as done for

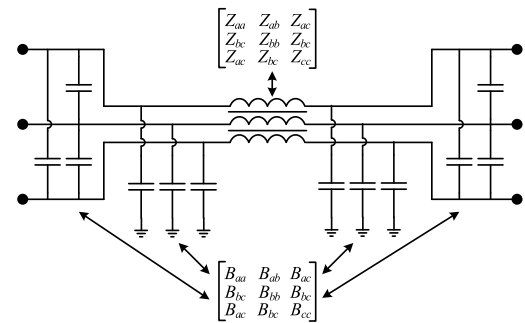


Fig. 11. Model implementation of a distribution feeder section.

transmission line section 100–101 for separation between cores 1 and 2, and ARTEMiS Stubline block for the rest of separation points.

The ARTEMiS Stubline block, modeled based on [23], implements an N-phase distributed parameters transmission line model with exactly one time step propagation delay. Therefore, it permits the decoupling of state-space system equations of networks on its both sides. Model splitting at distribution feeder sections 816–824, 854–852, 858–834, 701–702, 713–704, 703–730, and 733–734, are

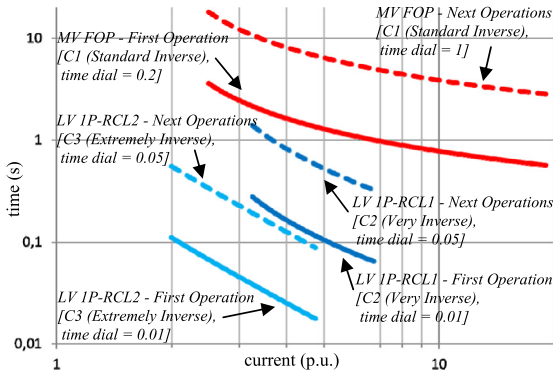


Fig. 12. Selected curves for MV feeder protective relay and LV reclosers.

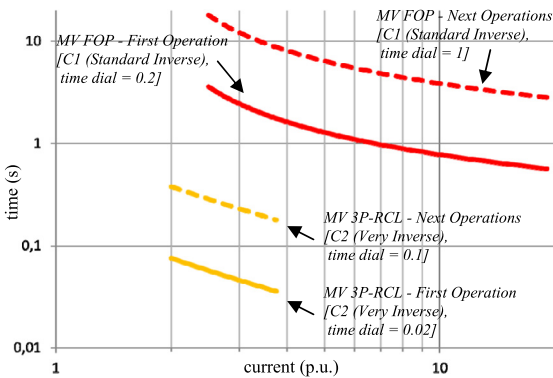


Fig. 13. Selected curves for MV feeder protective relay and MV recloser.

done by modeling part of these feeder sections by Stubline blocks. The principle to do such a modeling is to deduct part of the feeder impedance equally from all three phases such that the deducted part represents a balanced line section and it can be modeled by a Stubline block.

The Stubline block can also be used in combination with a transformer model to form a component called Stubline Transformer. The Stubline Transformer exhibits a decoupling delay between its primary and secondary sides. The principle to build such a component is to move the secondary winding leakage inductance and resistance to a Stubline block which is in series with the winding itself. Using this principle, model splitting at transformer sections 104–106 and 832–888 is done by Stubline Transformer blocks.

Fig. 14 illustrates the above-mentioned methods used for splitting the grid model.

4.2. Sample real-time simulation results

Figs. 15–25 show sample real-time simulation results for a test scenario where all dynamic loads (total of 260 kVA) are switched on at $t = 30$ s and a 6-cycle three-phase fault occurs on the MV feeder at node 858 (shown in Fig. 10) at $t = 50$ s. The figures include system frequency, system voltage at a number of selected nodes, tap changing operation of voltage regulators, power transfer between different voltage levels, three-phase recloser operation, power output of a number of selected distributed generators such as wind farm, PV systems and CES system together with its battery SoC, and rotor speed and current of a couple of dynamic loads. The simulation sample time in this study was fixed time step of $50 \mu\text{s}$.

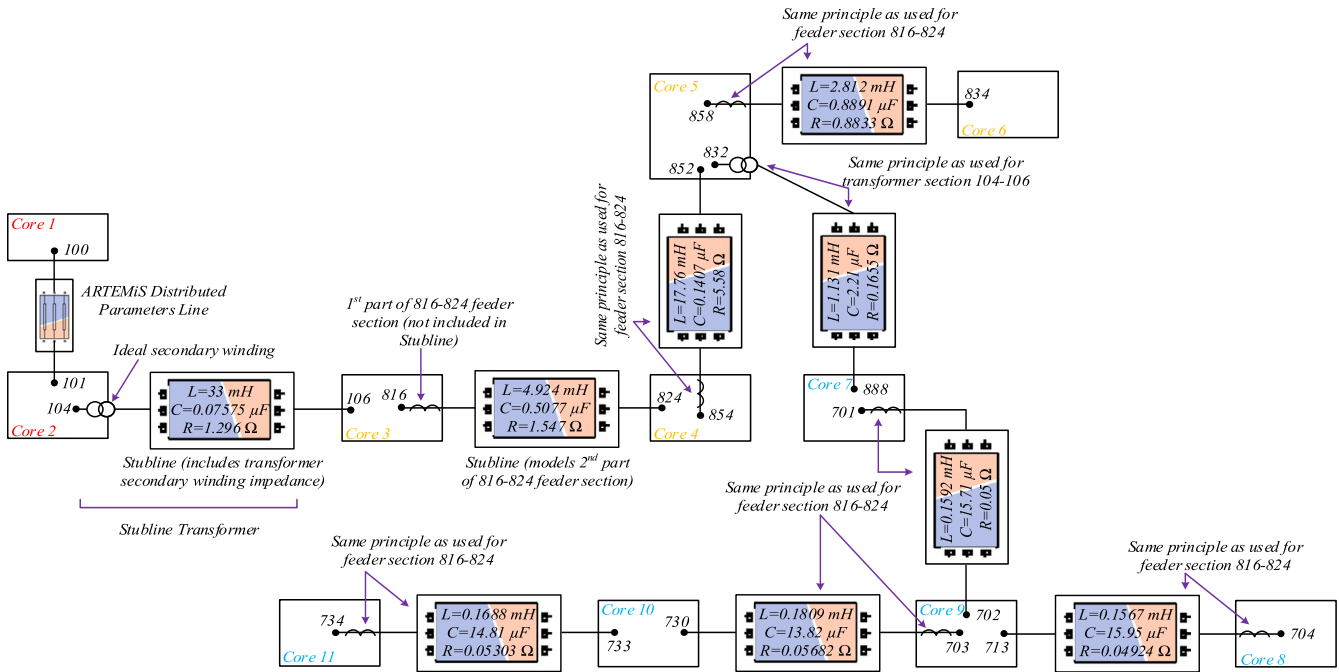


Fig. 14. Splitting of the grid model to allow process parallelization.

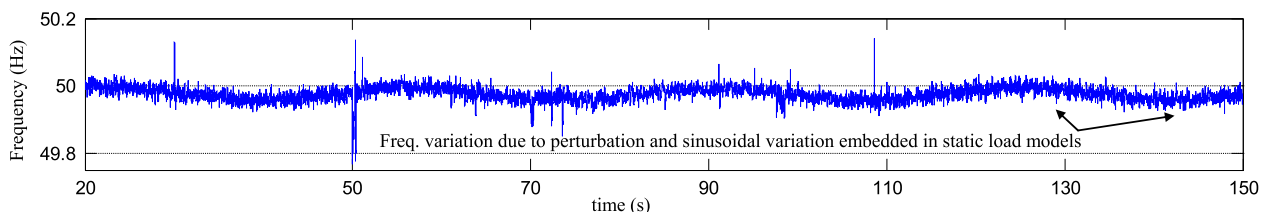


Fig. 15. Real-time simulation results—system frequency.

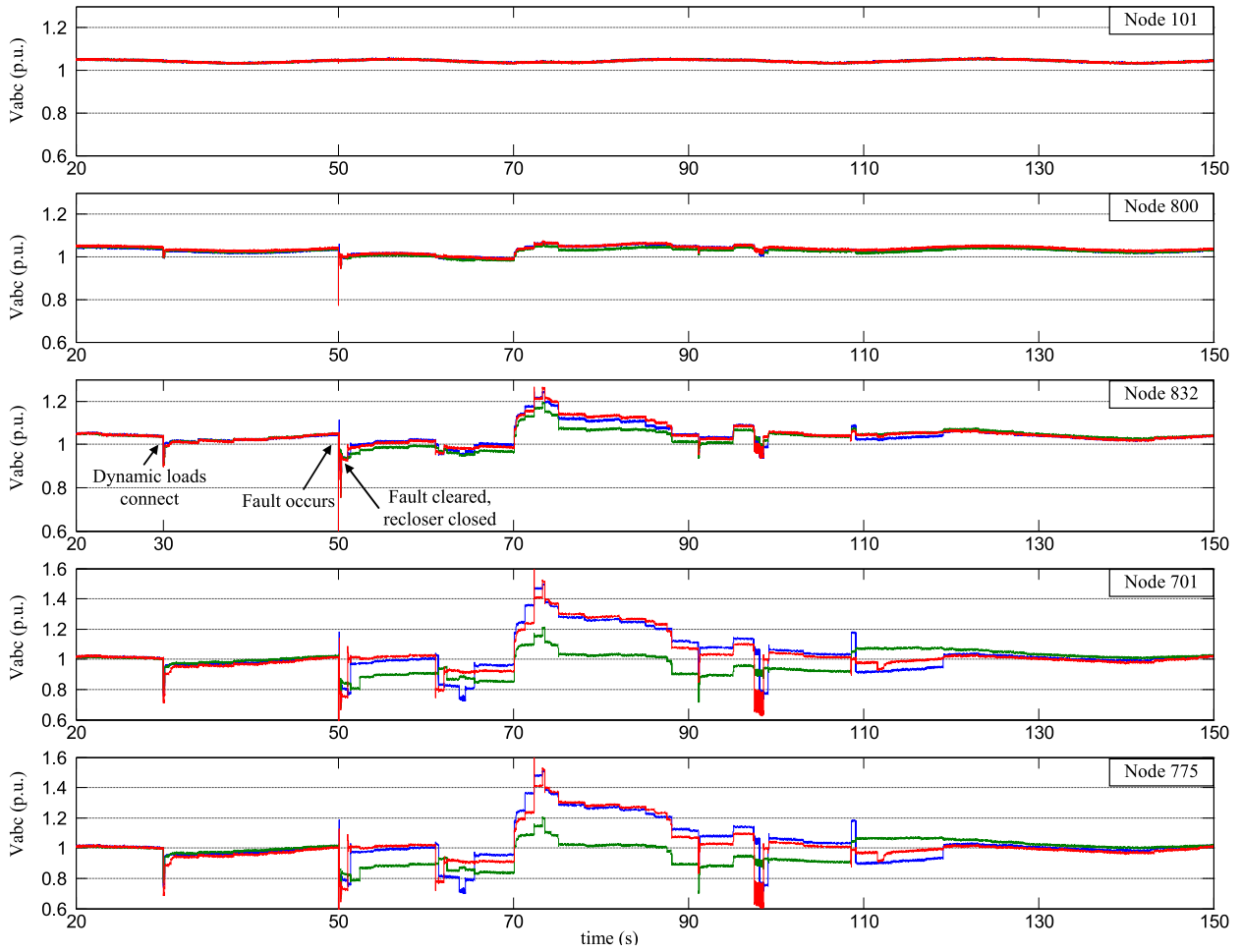


Fig. 16. Real-time simulation results—system voltages (Phase 'a' — Phase 'b' — Phase 'c' —).

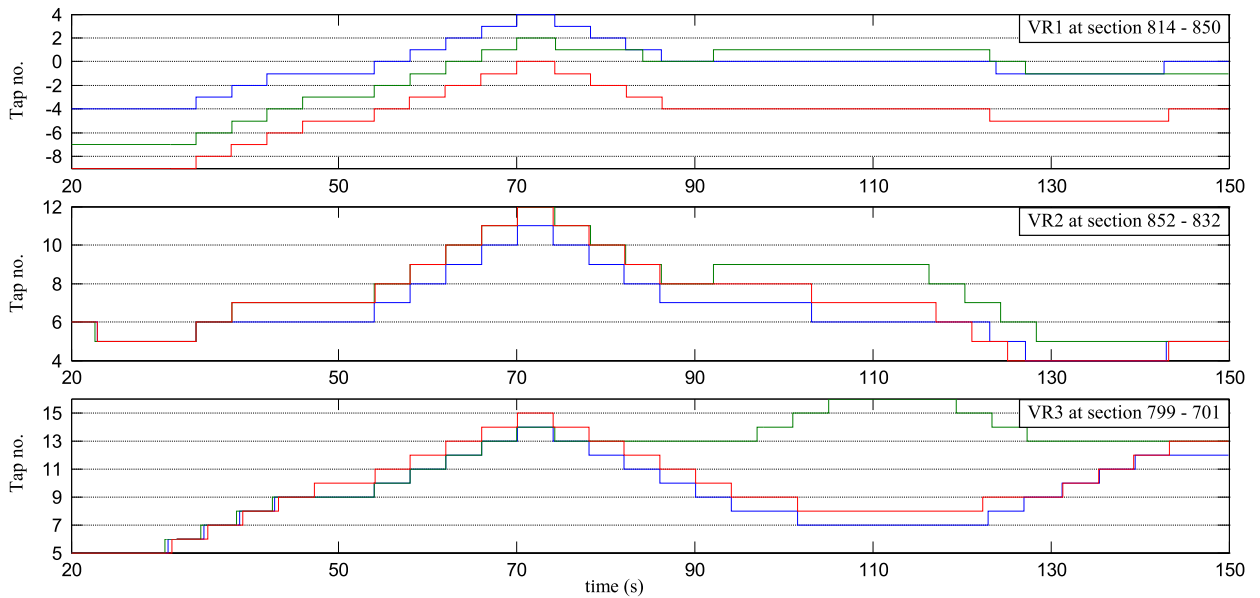


Fig. 17. Real-time simulation results—tap position of voltage regulators (Phase 'a' — Phase 'b' — Phase 'c' —).

As shown in Figs. 15 and 18, the random perturbation and sinusoidal variation embedded in static load models are clearly visible in the measured frequency and the power transferred from the EPS component to the HV section of the grid. After the fault occurrence

at $t = 50$ s, the three-phase MV recloser detects and isolates the fault within 2 cycles as shown in Fig. 19. The fault clears during the first open interval of the recloser. As shown in Fig. 18, due to insufficient voltage support after the fault, a sequence of discon-

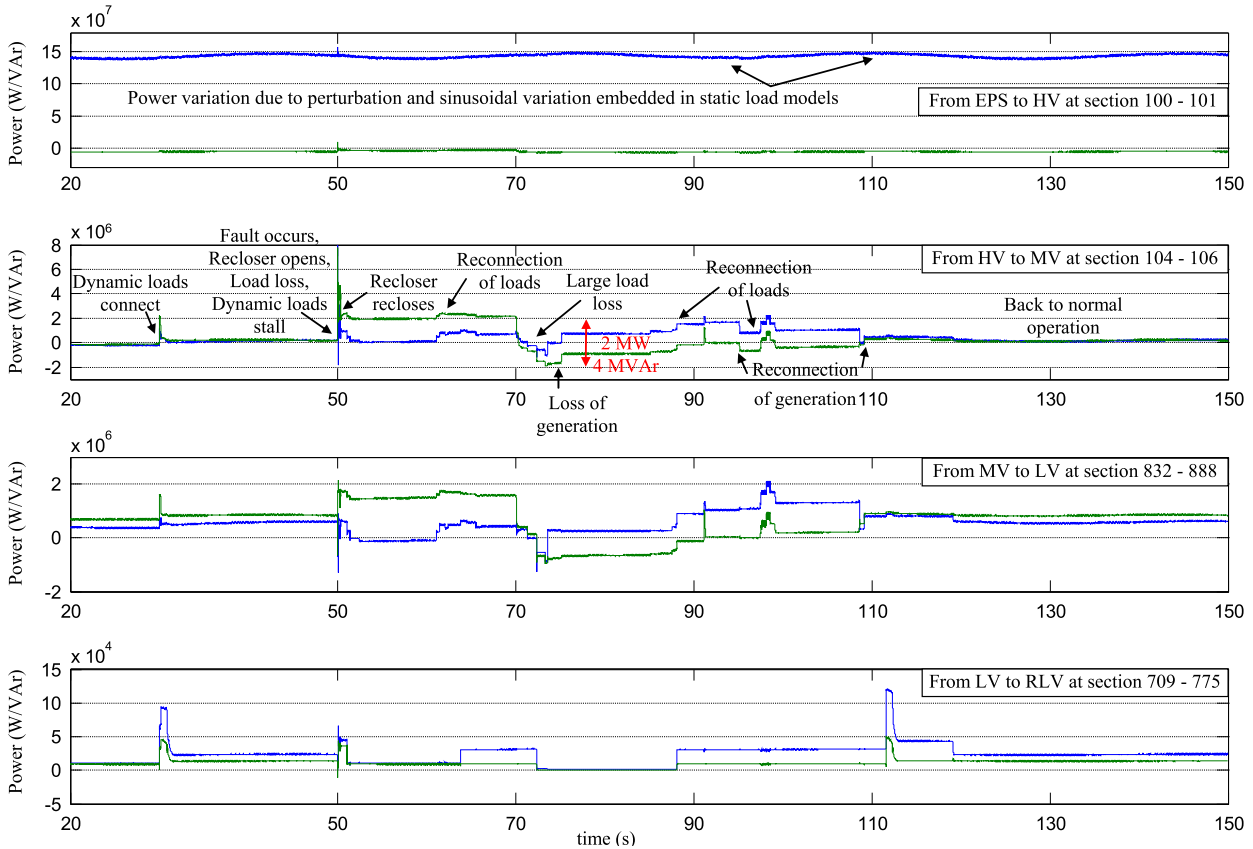


Fig. 18. Real-time simulation results—power transfer between different voltage levels (Active power — Reactive power —).

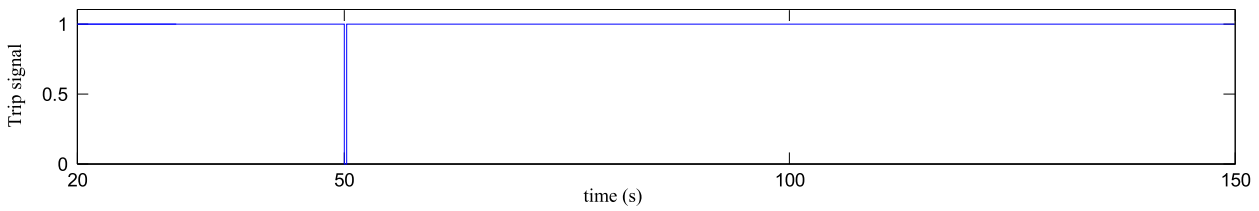


Fig. 19. Real-time simulation results—three-phase recloser operation at section 832–858.

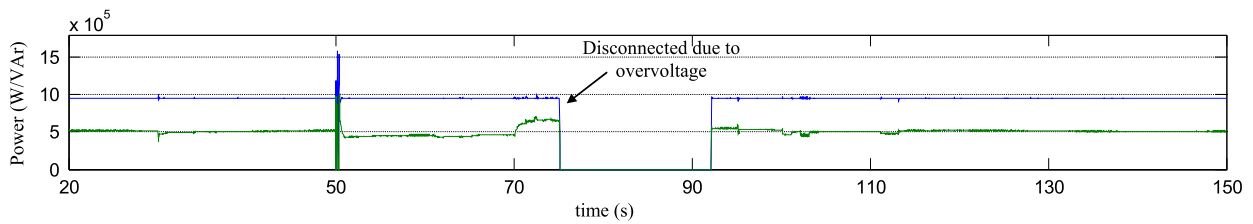


Fig. 20. Real-time simulation results—wind farm power generation at node 840 (Active power — Reactive power —).

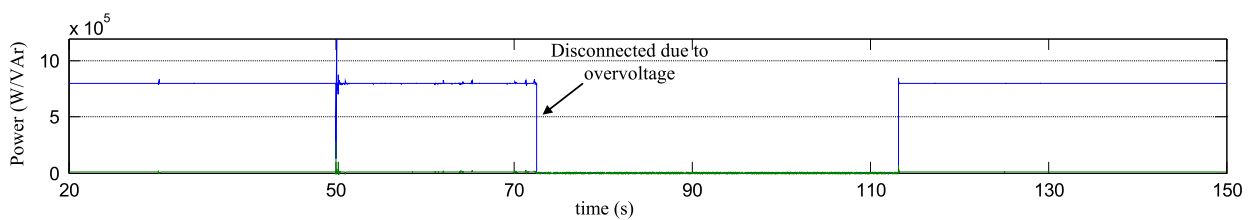


Fig. 21. Real-time simulation results—PV farm power generation at node 701 (Active power — Reactive power —).

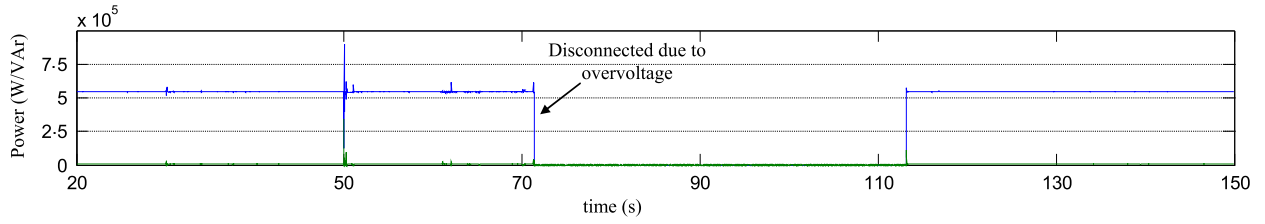


Fig. 22. Real-time simulation results—residential PV system power generation at node 703 (Active power — Reactive power —).

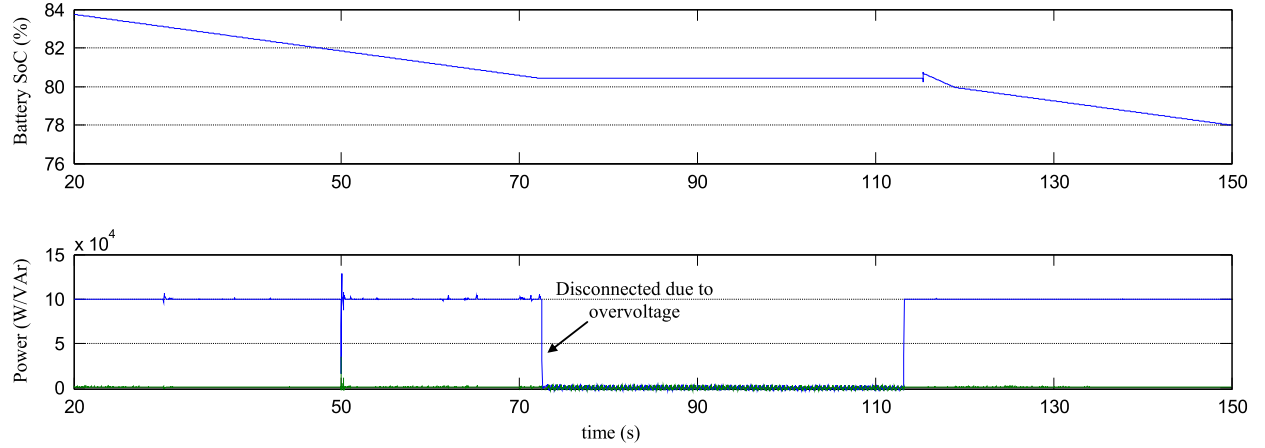


Fig. 23. Real-time simulation results—CES system power generation and battery SoC at node 724 (Active power — Reactive power —).

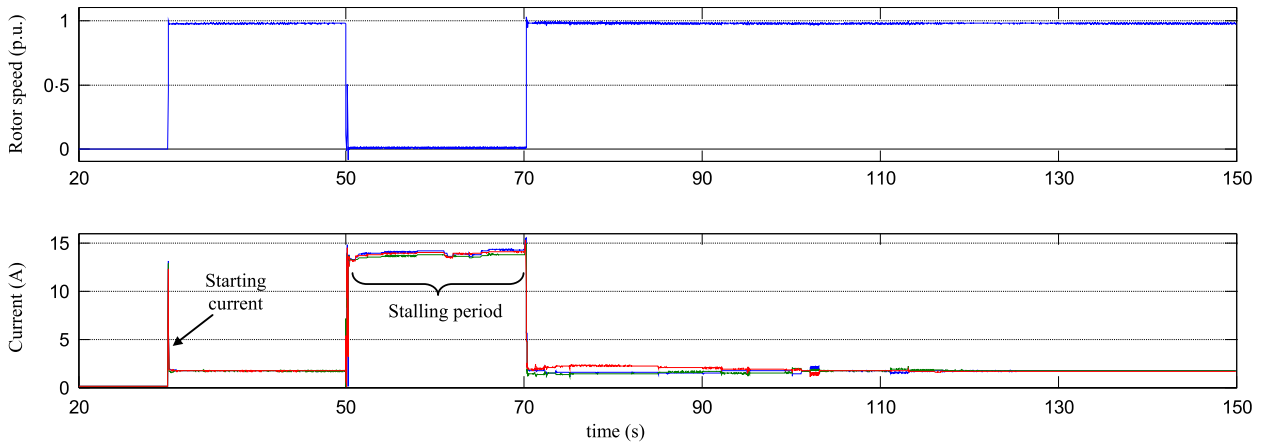


Fig. 24. Real-time simulation results—three-phase dynamic load rotor speed and current at node 860 (Phase 'a' — Phase 'b' — Phase 'c' —).

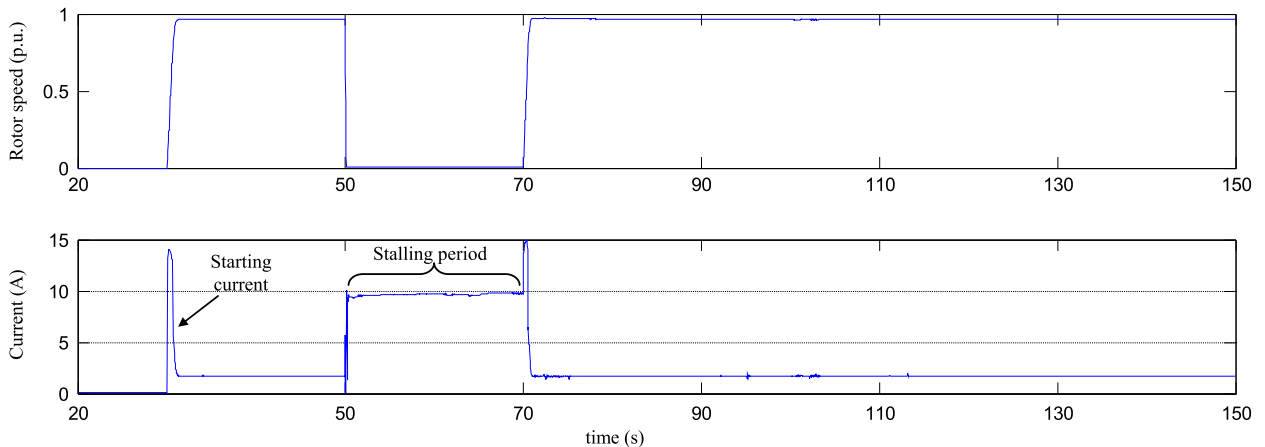


Fig. 25. Real-time simulation results—single-phase dynamic load rotor speed and current at node 848.

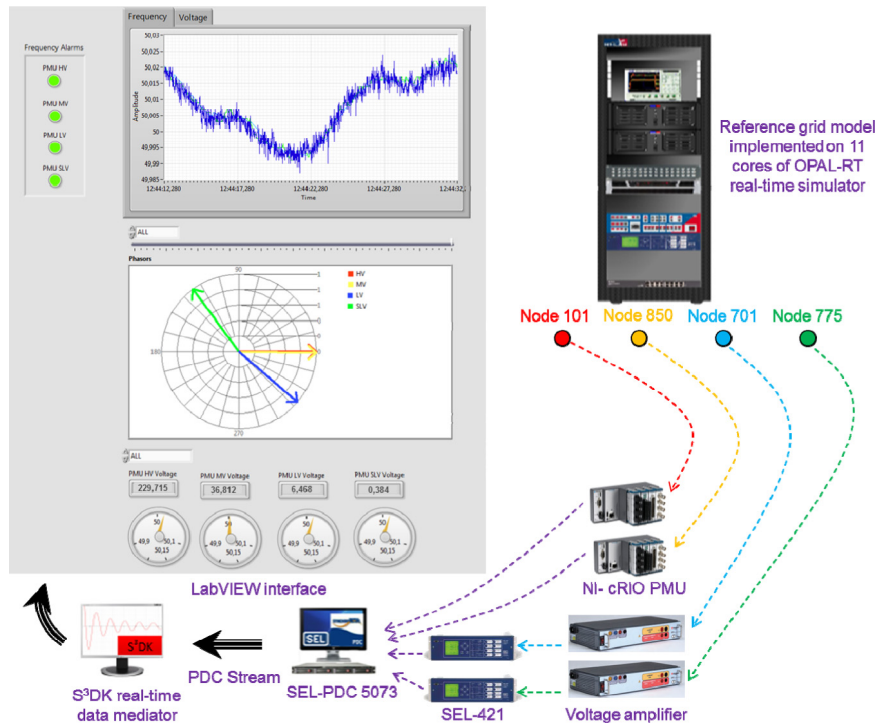


Fig. 26. Hardware-in-the-loop setup and LabVIEW interface prepared for monitoring the reference distribution grid model via PMU measurements. (For interpretation of the references to color in this figure legend, the reader is referred to the web version of this article.)

nection and reconnection of loads and distributed generation occur before the grid returns to its normal operation. These events noticeably affect the system voltage as shown in Fig. 16. For example, gradual reconnection of static loads after $t = 60$ s plus stalling of dynamic loads (which started right after the fault occurrence at $t = 50$ s) cause the system voltage to drop, as depicted in Fig. 16. At $t = 70$ s, a large load loss occurs due to insufficient voltage support, especially in the LV section. As a consequence, the reactive power, injected by capacitor banks at nodes 702 and 730 in the LV section, is not absorbed by the loads and flows to the MV section, as shown in the third plot of Fig. 18. This extra reactive power results in a noticeable system overvoltage during the period of $t = 70$ s to $t = 90$ s.

It is worth noting that, as highlighted in Fig. 18, such sequence of events in an active distribution grid like the modeled reference distribution grid can result in noticeable unexpected variation of power flow, in this case 2 MW (≈ 0.66 p.u.) and 4 MVar (≈ 1.33 p.u.) change in the power flowing from the HV section to the MV section. Such sudden demand variations imply the need for tighter operation and coordination of the transmission and distribution grids' operators.

4.3. Hardware-in-the-loop setup

Fig. 26 shows the hardware-in-the-loop setup for grid monitoring via PMU measurements. As shown, four measurement locations at different voltage levels have been specified on the grid model. The measured voltages are fed to PMUs through the analogue output ports of the OPAL-RT simulator. As indicated in the figure, two PMUs used in this setup are Compact Reconfigurable IO systems (CRIO) from National Instruments Corporation, programmed with LabVIEW graphical programming tools to perform phasor calculations [24]. The other two PMUs are SEL-421 from Schweitzer Engineering Laboratories, being fed through a voltage amplifier. This is because the rated voltage of SEL-421 input is 300 V, making it suitable for commercial applications; hence, it is

Table 9
Parameters of transmission line sections.

Node A	Node B	Length (km)	[R1 R0] (Ω/km)	[L1 L0] (mH/km)	[C1 C0] ($\mu\text{F}/\text{km}$)
100	101	15			
101	102	45			
101	102	45			
101	103	151	[0.2412	[4 12.1]	[0.0017
101	103	151	0.7237]		0.0051]
102	104	50			
103	104	50			
104	105	50			

Table 10
Parameters of transformers.

Segment	MVA	kV LL-high	kV LL-low	R (%)	X (%)
104–106	5	230-D	36-Gr. W	1	8
832–888	2.5	36-Gr.W	6.6-Gr. W	1.9	4.08
709–775	0.5	6.6-Gr.W	0.4-Gr. W	0.09	1.81

Table 11
Parameters of capacitor banks.

Node	Ph-A (kVAr)	Ph-B (kVAr)	Ph-C (kVAr)
844	100	100	100
848	150	150	150
702	250	50	250
730	100	–	150

much higher than the rated voltage of the simulator analogue output which is 16 V.

The PMU data are then sent to a PDC which streams the data over TCP/IP to a workstation computer holding Statnett's Synchrophasor Development Kit (S³DK) [25], which provides a real-time data mediator that parses the PDC data stream and makes it available to the user in the LabVIEW environment. Utilizing functions provided by the S³DK, an interface was developed

Table 12
Parameters of single-phase step voltage regulators.

Regulator ID	Line segment	Location	Connection	Monitoring phase	S_n (MVA)	V_n (kV L-G)	I_n (A)
1	814–850	814	3-Ph, LG	A–B–C	5	20	200
2	852–832	852	3-Ph, LG	A–B–C	5	20	200
3	799–701	799	3-Ph, LG	A–B–C	2.5	3.8	350

Regulator ID	V_{ref} (p.u.)	BW (p.u.)	R_{comp} (V)	X_{comp} (V)
1	1.0167	0.016	2.7	1.6
2	1.0334	0.016	2.5	1.5
3	1.0167	0.016	1.5	3

Table 13
Parameters of static loads.

Node	Type	P_{n-a} (kW)	Q_{n-a} (kVAr)	P_{n-b} (kW)	Q_{n-b} (kVAr)	P_{n-c} (kW)	Q_{n-c} (kVAr)
101	Y-PQ	6670	0	6670	0	6670	0
102	Y-PQ	28330	0	28330	0	28330	0
103	Y-PQ	13330	0	13330	0	13330	0
104	Y-PQ	6670	0	6670	0	6670	0
105	Y-PQ	6670	0	6670	0	6670	0
860	D-Z	16	8	20	10	110	55
840	Y-I	9	7	9	7	9	7
840	D-I	18	9	22	11	0	0
844	Y-Z	135	105	135	105	135	105
844	Y-PQ	9	5	0	0	0	0
848	D-PQ	20	16	20	16	20	16
830	D-Z	10	5	10	5	25	10
806	Y-PQ	0	0	30	15	25	14
810	Y-I	0	0	16	8	0	0
820	Y-Z	34	17	0	0	0	0
822	Y-PQ	135	70	0	0	0	0
824	D-I	0	0	5	2	0	0
826	Y-I	0	0	40	20	0	0
828	Y-PQ	0	0	0	0	4	2
856	Y-PQ	0	0	4	2	0	0
858	D-Z	7	3	2	1	6	3
864	Y-PQ	2	1	0	0	0	0
834	D-PQ	4	2	15	8	13	7
836	D-PQ	30	15	10	6	42	22
838	Y-PQ	0	0	28	14	0	0
846	Y-PQ	0	0	25	12	20	11
701	D-PQ	140	70	140	70	350	175
712	Y-PQ	0	0	0	0	85	40
713	Y-PQ	0	0	0	0	85	40
714	D-I	17	8	21	10	0	0
718	Y-Z	85	40	0	0	0	0
720	Y-PQ	0	0	0	0	85	40
722	D-I	0	0	140	70	21	10
724	Y-Z	0	0	42	21	0	0
725	Y-PQ	0	0	42	21	0	0
727	Y-PQ	0	0	0	0	42	21
729	Y-I	42	21	0	0	0	0
730	Y-Z	0	0	0	0	85	40
731	Y-Z	0	0	85	40	0	0
732	Y-PQ	0	0	0	0	42	21
733	Y-I	85	40	0	0	0	0
734	Y-PQ	0	0	0	0	42	21
735	Y-PQ	0	0	0	0	85	40
736	Y-Z	0	0	42	21	0	0
737	Y-I	140	70	0	0	0	0
738	Y-PQ	126	62	0	0	0	0
740	Y-PQ	0	0	0	0	85	40
741	Y-I	0	0	0	0	42	21
742	D-Z	8	4	85	40	0	0
744	Y-PQ	42	21	0	0	0	0
775	Y-PQ	10	3	10	3	10	3

Table 14
Parameters of dynamic loads.

Node	Connection	S_n (kVA)	V_n (kV-LL)
830	Phase 'a'	7.6	36
848	Phase 'b'	25.5	36
860	3-Ph	76.8	36
728	3-Ph	140	6.6
775	Phase 'c'	10	0.4

Table 15
Parameters of wind farms.

Node	N_{WT}	V_n (kV-LL)	Type	W_c (m/s)
105	33	230	Constant	15
854	1	36	Constant	10
840	1	36	Constant	10

Table 16
Parameters of PV farms.

Node	N_{PV}	V_n (kV-LL)	Type	SI_c (W/m ²)
701	8	6.6	Constant	1000
730	4	6.6	Constant	625

Table 17
Parameters of residential PV systems.

Node	Connection	N_{PV}	V_n (kV-LL)	Type	SI_c (W/m ²)
703	Phase 'c'	55	6.6	Constant	1000
708	Phase 'a'	20	6.6	Constant	1000
775	Phase 'a'	2	0.4	Constant	1000

Table 18
Parameters of CES systems.

Node	S_{inv} (kVA)	V_n (kV-LL)	Ah
724	150	6.6	195
741	100	6.6	130

using LabVIEW. The LabVIEW interface displays the time-stamped frequency and voltage data on a diagram and the voltage phasors on a phasor pane. There are also lamp signals, functioning as alarms, which change color if the measured frequency goes beyond the permissible range.

This is the basic platform that will be used to develop PMU-based monitoring applications for TSO/DSO interaction through dynamic information exchange.

5. Conclusions and future work

This paper presented a distribution grid model, specified, implemented and simulated to serve as a benchmark for dynamic performance studies within the IDE4L project. Various component models were developed and incorporated in the grid model. The model was simulated in real-time using the OPAL-RT simulator and was utilized in a hardware-in-the-loop setup to develop grid monitoring applications that exploit PMU measurements.

As future work, the reference grid model will be implemented in another software platform for validation of the results that are obtained from the MATLAB/Simulink implementation. Also, the

algorithms, to be developed during the IDE4L project, for exchange of key dynamic information between TSOs and DSOs will be added to this setup for evaluation and demonstration purposes.

Appendix A

A.1. Parameters of transmission line sections

See Table 9.

A.2. Parameters of transformers

See Table 10.

A.3. Parameters of shunt capacitor banks

See Table 11.

A.4. Parameters of single-phase step voltage regulators

f_n and T_d of all VRs are set as listed in Table 1.
See Table 12.

A.5. Parameters of static loads

V_n of loads connected to nodes from 860 to 846, from 701 to 744, and 775 are 36 kV L–L, 6.6 kV L–L, and 0.4 kV L–L, respectively.

f_n , V_{omv} , load change parameters, and protecting settings of static loads are set as listed in Table 2.

See Table 13.

A.6. Parameters of dynamic loads

All other parameters of dynamic loads are set as listed in Table 3.
See Table 14.

A.7. Parameters of wind farms

All other parameters of wind farms are set as listed in Table 4.
See Table 15.

Table 19
Parameters of feeder overcurrent protection relays.

Segment	$T_{interval}$	Curve	First operation		Next operations	
			$I_{pick-up}$	TD	$I_{pick-up}$	TD
106–800	[0.25 15 35]	Phase relay	140	0.2	140	1
		Ground relay	100	0.2	100	1

Table 20
Parameters of 3-phase recloser.

Segment	$T_{interval}$	Connection	Curve	First operation		Next operations	
				$I_{pick-up}$	TD	$I_{pick-up}$	TD
832–858	[0.2 10 13]	One 3-Ph	Phase relay	35	0.02	35	0.1
			Ground relay	30	0.02	30	0.1

Table 21
Parameters of 1-phase reclosers.

Segment	$T_{interval}$	Connection	Curve	First operation		Next operations	
				$I_{pick-up}$	TD	$I_{pick-up}$	TD
890/799–701 730–709	[0.2 10 13]	Three 1-Ph	Phase relay	480	0.01	480	0.05
			Phase relay	155	0.01	155	0.05

A.8. Parameters of PV systems

All other parameters of PV systems are set as listed in Table 5. See Tables 16 and 17.

A.9. Parameters of CES Systems

All other parameters of CES systems are set as listed in Table 6. See Table 18.

A.10. Parameters of FOP, single- and three-phase reclosers

f_n for all protective components is set as 50 Hz. See Tables 19–21.

A.11. Parameters of EPS

All parameters of EPS are set as listed in Table 8.

Appendix B. Supplementary data

Supplementary material related to this article can be found online at <http://dx.doi.org/10.1016/j.segan.2015.06.002>. The attached .zip file contains two different versions of the model as of September 1st 2016. The latest versions of the model are available online at <https://github.com/SmarTS-Lab/FP7-IDE4L-KTHSmarTSLab-ADN-RTModel>.

References

- [1] EU-FP7 IDE4L project official website at: <http://www.ide4l.eu>.
- [2] Available online at: <http://www.ewh.ieee.org/soc/pes/dsacom/testfeeders/index.html>.
- [3] W.H. Kersting, A comprehensive distribution test feeder, in: Proc. IEEE PEST&D Conf., 2010.
- [4] J.S. Xavier, D. Das, Impact of network reconfiguration on loss allocation of radial distribution system, IEEE Trans. Power Deliv. 22 (4) (2007) 2473–2480.
- [5] W.H. Kersting, Distribution feeder voltage regulation control, IEEE Trans. Ind. Appl. 46 (2) (2010) 620–626.
- [6] T.V. Cutsem, C. Vournas, Voltage Stability of Electric Power Systems, Springer, 1998, p. 95.
- [7] B. Lesieutre, D.N. Kosterev, J. Undrill, Phasor modeling approach for single phase A/C motors, in: Proc. IEEE PES Conversion & Delivery of Electrical Energy in the 21st Century, 2008.
- [8] P.C. Krause, O. Wasynczuk, S.D. Sudhoff, Analysis of Electric Machinery, IEEE Press, 2002.
- [9] C. Dufour, J. Bélanger, A real-time simulator for doubly fed induction generator based wind turbine applications, in: Proc. IEEE 35th Annual Power Electronics Specialists Conference, 20–25 June 2004.
- [10] S. Heier, Grid Integration of Wind Energy Conversion Systems, John Wiley & Sons Ltd., 1998.
- [11] R. Pena, J.C. Clare, G.M. Asher, Doubly fed induction generator using back-to-back PWM converters and its application to variable-speed wind-energy generation, in: Proc. IEE Electric Power Applications, May 1996.
- [12] H. Hooshyar, M.E. Baran, Fault analysis on distribution feeders with high penetration of PV systems, IEEE Trans. Power Syst. 28 (3) (2013) 2890–2896.
- [13] IEEE recommended practice for utility interface of photovoltaic (PV) systems, IEEE 929, 2000.
- [14] O. Tremblay, L.A. Dessaint, Experimental validation of a battery dynamic model for EV applications, World Electr. Veh. J. 3 (2009).
- [15] L. Xu, Z. Miao, L. Fan, Control of a battery system to improve operation of a microgrid, in: Proc. IEEE PES General Meeting, 2008.
- [16] S.H. Horowitz, A.G. Phadke, Power System Relaying, third ed., Wiley, New York, 2008.
- [17] IEEE committee report, Dynamic models for steam and hydro turbines in power system studies, IEEE Trans. Power Appar. Syst. 92 (6) (1973) 1904–1915.
- [18] Recommended practice for excitation system models for power system stability studies, IEEE Standard 421.5, August 1992.
- [19] P. Kundur, Power System Stability and Control, McGraw-Hill, 1994.
- [20] R. Billinton, S. Kumar, N. Chowdhury, K. Chu, K. Debnath, L. Goel, E. Khan, P. Kos, G. Nourbakhsh, J. Oteng-Adjei, A reliability test system for educational purposes—basic data, IEEE Trans. Power Syst. 4 (3) (1989) 1238–1244.
- [21] CIGRE Benchmark systems for network integration of renewable and distributed energy resources, CIGRE Task Force C6.04.02, May 2013.
- [22] H.B. Funmilayo, J.A. Silva, K.L. Butler-Purry, Overcurrent protection for the IEEE 34-node radial test feeder, IEEE Trans. Power Deliv. 27 (2) (2012) 459–468.
- [23] H. Dommel, Digital computer solution of electromagnetic transients in single and multiple networks, IEEE Trans. Power Appar. Syst. PAS-88 (4) (1969) 388–399.
- [24] Available online at: <http://sine.ni.com/nips/cds/view/p/lang/sv/nid/210502>.
- [25] L. Vanfretti, V.H. Aarstrand, M.S. Almas, V.S. Peric, J.O. Gjerde, A software development toolkit for real-time synchrophasor applications, in: Proc. IEEE PowerTech, 2013.